In: J. W. Lukaszewicz & P. Niemcewicz (eds.), Proceedings of the 11th International Congress on Deterioration and Conservation of Stone, 15–20 September 2008, Torun, Poland, Volume I, p. 597–604.

# DOLOMITIC LIME MORTAR – A COMMONLY USED BUILDING MATERIAL FOR MEDIEVAL BUILDINGS IN WESTERN AUSTRIA AND NORTHERN ITALY

A. Diekamp[1*], J. Konzett[1], W. Wertl[1], R. Tessadri[1], P.W. Mirwald[1]
[1]*Institute of Mineralogy and Petrography, University of Innsbruck, Austria*

**Abstract**

Plaster and mortar samples have been collected from buildings in Northern Tyrol/Austria and Southern Tyrol/Italy representing the periods from Romanesque to Baroque. The mineralogical composition and the textures of the binding material of these plasters and mortars were studied. One of the most important results is the discovery of dolomitic lime mortars at most localities investigated.

Magnesite, hydromagnesite and brucite could be identified using a combination of XRD, DTA/TG, EMPA, Raman spectroscopy. In addition X-ray mapping and DTA/TG analysis indicate the presence of amorphous or poorly crystalline magnesium phases.

**Keywords:** historic mortar, dolomitic lime, magnesium phases, hydromagnesite, magnesite, brucite.

## 1. Introduction

In Northern Tyrol/Austria and Southern Tyrol/Italy, many medieval buildings still exist where Romanesque and Gothic plasters and mortars have been preserved. Many are still in an amazingly pristine state of preservation in spite of the harsh Alpine climate. As part of an EU-Interreg project, the mineralogical composition and the textures of these plasters and mortars were studied. One of the most important results of this study is the discovery of dolomitic lime mortars at 19 out of 25 localities investigated. This shows that in this region, dolomite is a much more common constituent of plasters and mortars than previously assumed. The formation of magnesium phases from MgO during setting is considered to be a major cause of the exceptional durability of these building materials.

Firing of dolomitic limestone results in the formation of CaO and MgO, both of them highly reactive during subsequent slaking, leading to the formation of portlandite $Ca(OH)_2$ and brucite $Mg(OH)_2$. In contrast to portlandite that reacts to $CaCO_3$ during setting in a sufficiently $CO_2$-rich environment, the formation of $MgCO_3$ is delayed or inhibited in favour of the formation of hydrous magnesium phases such as hydromagnesite $4MgCO_3 \cdot Mg(OH)_2 \cdot 4H_2O$, nesquehonite $MgCO_3 \cdot 3H_2O$, artinite $MgCO_3 \cdot Mg(OH)_2 \cdot 3H_2O$ and brucite $Mg(OH)_2$ (Siedel et al. 2003b), a process controlled by the water content of the mortar and the $CO_2$ and moisture concentration of

* Corresponding author: anja.diekamp@uibk.ac.at

the atmosphere. In addition to these crystalline phases, amorphous magnesium phases may be present of which the characterisation is extremely difficult (Niesel and Schimmelwitz 1971, Montoya et al. 2003, Siedel et al. 2003a).

## 2. Analytical methods

A total of 254 plaster and mortar samples have been collected from 25 buildings (churches, castles, ruins in Northern and Southern Tyrol) representing the periods from Romanesque to Baroque. In most cases it was possible to collect from the individual object a number of samples accurately dated by art historians.

X-ray diffraction analysis (XRD): was performed on 254 crushed and sieved samples (sieve fraction < 0.063 mm with aggregates removed) in an attempt to characterize the mineralogical composition of the binder, using a SIEMENS D500 powder diffractometer with Bragg-Brentano optics.

Thermogravimetric analysis (DTA/TG): thermogravimetric and calorimetric analyses were performed on 154 samples with a simultaneous DTA/TG instrument (SETARAM SETSYS evolution 2400) using powdered sample material placed in a corundum crucible. A heating rate of 10 °C $min^{-1}$ in a helium atmosphere was applied. In order to correlate the weight loss observed during heating of the sample due to release of $H_2O$ and/or $CO_2$ as result of carbonate and hydroxyl phase breakdown, a Quadrupol mass spectrometer was coupled with the DTA/TG device.

In addition to XRD and DTA/TG the mineralogy and textures of a representative selection of the samples were investigated using polished thin sections and a petrographic microscope (Olympus BX40).

Identification and quantitative analysis of the mineral phases was carried out with electron microprobe analysis (EMPA, JEOL JXA 8100) in both energy and wave length dispersive analytical modes. Analytical conditions of 15 kV accelerating voltage and 10 or 5 nA beam current have been employed with variable spot sizes between 3 and 50 µm to minimize beam damage of the analyzed phases. To study element distribution with particular emphasis on the occurrence of magnesium, wavelength dispersive X-ray mapping was performed. In addition to quantitative and mapping analysis, the backscattered electron (BSE) imaging mode was used extensively to study mineral textures and assemblages on a micrometer scale.

In order to unambiguously identify phases containing OH and/or $CO_3$ characterized by only subtle differences in their stoichiometries, Raman spectroscopy (JOBIN-YVON LabRam HR800 with confocal optics) was used.

The three dimensional textures of magnesium phases was studied on broken surfaces using scanning electron microscopy (SEM).

## 3. Results

### 3.1 X-ray powder diffraction

In 33 % of the 254 investigated mortars and plasters at least one or usually several magnesium phases could be identified in the binding material as additional mineral phases to calcite. These phases are magnesite (26 %), hydromagnesite (17 %) and brucite (4.5 %). Neither nesquehonite nor artinite could be identified.

### 3.2 Differential Thermal Analysis

154 samples for which also XRD results are available were analysed using DTA/TG. In all cases where XRD shows magnesite, hydromagnesite or brucite, the DTA/TG measurements, too, yields unambiguous evidence for the presence of these phases.

However, while DTA/TG analysis provides evidence for the presence of magnesium phases in 60 % of the samples, this is only true for 40 % when XRD is considered only. Likely causes for this discrepancy will be discussed in section 4.

In a first step samples have been selected for combined DTA/TG-mass spectrometry analysis that contain significant amounts of a specific magnesium phase as documented by XRD results (Figs. 1-3). This strategy was chosen to unambiguously identify the DTA/TG signals of magnesite, hydromagnesit and brucite in a typical calcite bearing binder matrix and to detect ion current signals for $H_2O$ and $CO_2$ during the thermal breakdown of these phases.

In cases where mass loss can be assigned to a specific decarbonation or dehydration/dehydroxylation reaction, the relative proportions of the respective phases were calculated. It should be mentioned, however, that this method cannot be considered strictly quantitative due to a possible minor overlap of these two reactions as indicated by the ion current signals. Three examples for well interpretable DTA/TG experiments are described in the following:

Binder containing calcite and brucite (Fig. 1):

(1) endothermic reaction at 410 °C, due to release of $H_2O$ as a result of dehydoxylation of brucite, 12 % mass loss during reaction corresponding to 39 % brucite; (2) endothermic reaction at 740 °C, due to release of $CO_2$ as a result of decarbonation of calcite, 11 % mass loss during reaction corresponding to 26 % calcite. This results in a calcite : brucite ratio of 1 : 1.5.

Binder containing calcite and hydromagnesite (Fig. 2):

(1) endothermic reaction at 262 °C, due to release of $H_2O$ and (2) endothermic reaction at 371 °C, due to release of $H_2O$ and $CO_2$ as a result of a two step thermal decomposition of hydromagnesite to $MgCO_3$, $H_2O$ and $CO_2$; (3) endothermic reaction at 452 °C, due to release of $CO_2$ as a result of decarbonation of $MgCO_3$; (4) endothermic reaction at 740 °C, due to release of $CO_2$ as a result of decarbonation of calcite, 18 % mass loss during reaction corresponding to 40 % calcite.

Binder containing calcite and magnesite (Fig. 3):

(1) endothermic reaction at 550 °C, due to release of $CO_2$ as a result of decarbonation of magnesite, 21 % mass loss during reaction corresponding to 41 % magnesite; (2) endothermic reaction at 760 °C, due to release of $CO_2$ as a result of decarbonation of calcite, 24 % mass loss during reaction corresponding to 55 % calcite. This results in a calcite : magnesite ratio of 1 : 0.75.

While in the three samples presented above the magnesium phases can be identified solely based on the DTA signals, in the majority of the investigated samples only a combination of DTA signals with ion currents allows the identification of magnesium phases or, at least, yield hints for their presence.

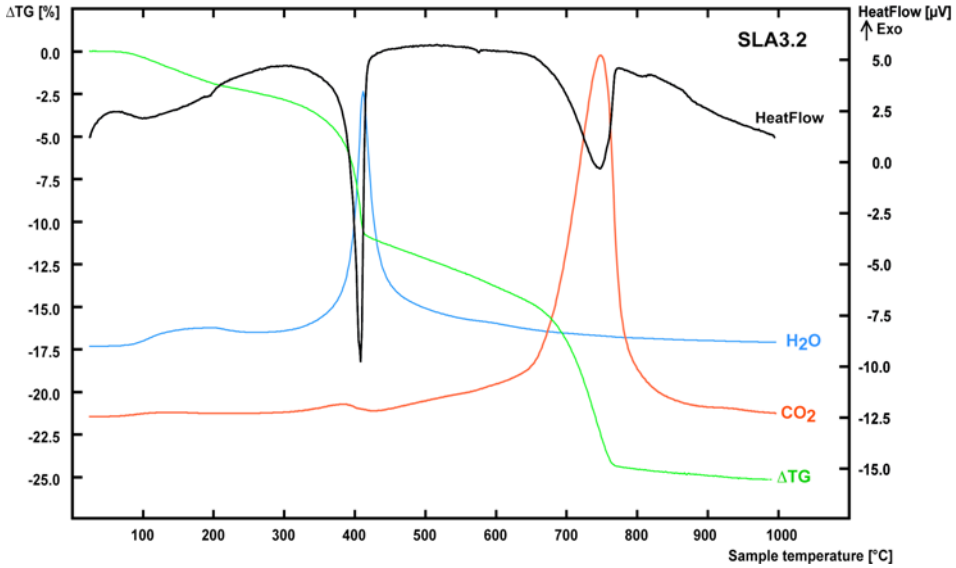


Figure 1: DTA/TG-curves for binder containing calcite and brucite (Landeck castle, excavation, sample SLA3.2); note that the ion currents for $CO_2$ and $H_2O$ are not calibrated quantitatively an only serve to identify the species liberated.

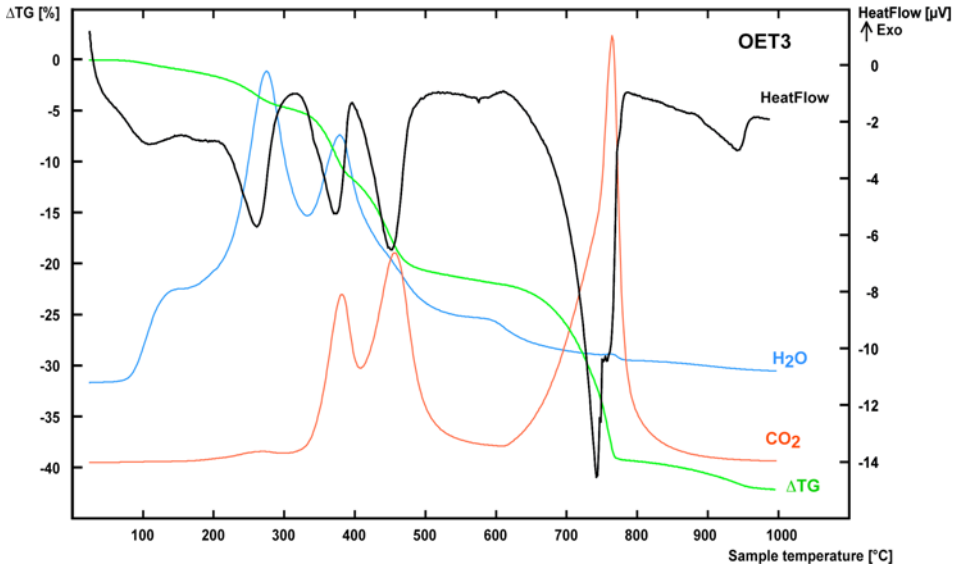


Figure 2: DTA/TG-curves for binder containing calcite and hydromagnesite (Tower of Oetz, sample OET3); meaning of $CO_2$ and $H_2O$ signals as in Fig. 1.

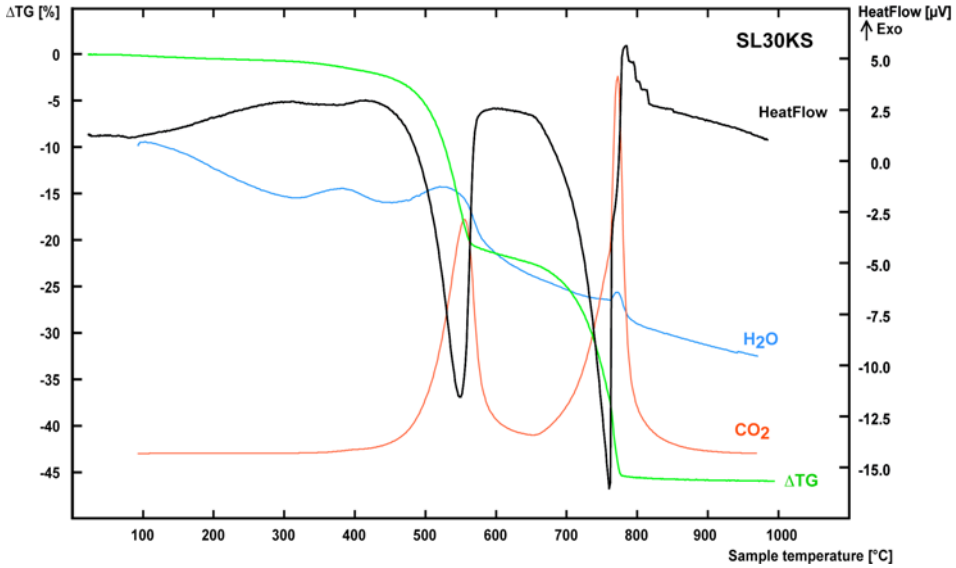


Figure 3: DTA/TG-curves for binder containing calcite and magnesite (Landeck castle, sample SL30KS); meaning of $CO_2$ and $H_2O$ signals as in Fig. 1.

### 3.3 Optical and spectroscopic methods

Three types of textures indicative of the presence of magnesium phases could be identified: (1) diffuse brownish patches within the binder up to several hundred µm in diameter and visible with the petrographic microscope (Fig. 4a). The BSE imaging mode shows these areas to be denser than the surrounding binder (Fig. 4b). EMP-analysis of these dense areas in Fig. 4b shows a composition of 20–28 % MgO, 14–17 % CaO, < 1.5 % $SiO_2$ and < 1.0 % FeO. Elemental mapping reveals an intimate intergrowth of calcium and magnesium phases - the former most likely calcite - that are too small to be unambiguously identified. Fig. 4c shows an elemental mapping of the magnesium in a binder area. (2) Radial aggregates of fibrous anisotropic phases of a size in the range 50-250 µm (Figs. 5a and 5b). SEM-imaging on broken surfaces shows that these aggregates consist of intergrown fine platelets forming globular aggregates (Fig. 5c). Both EMP-analysis and Raman spectroscopy reveal that these platelets are hydromagnesite. (3) Hydromagnesite may also be present as linings growing into open cracks and pores (Figs. 5d and 5f) or covering the surface of plasters (Fig. 5e).

SEM-textures of hydromagnesite and amorphous/poorly crystalline magnesium phases typically show interlocking crystal aggregates.

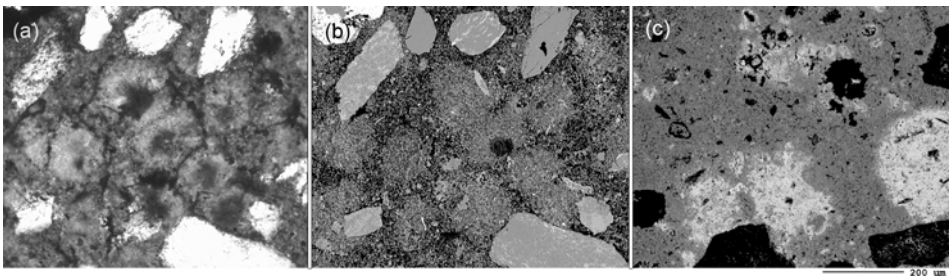


Figure 4: Examples of magnesium enriched areas in dolomitic lime mortars. (a) thin section photomicrograph of diffuse brownish patches in the binder; parallel polarizers, field of view 1.04 mm across; (b) the same area: EMPA photomicrograph in BSE imaging mode; (c) EMPA elemental mapping of magnesium (brighter areas are enriched in magnesium)

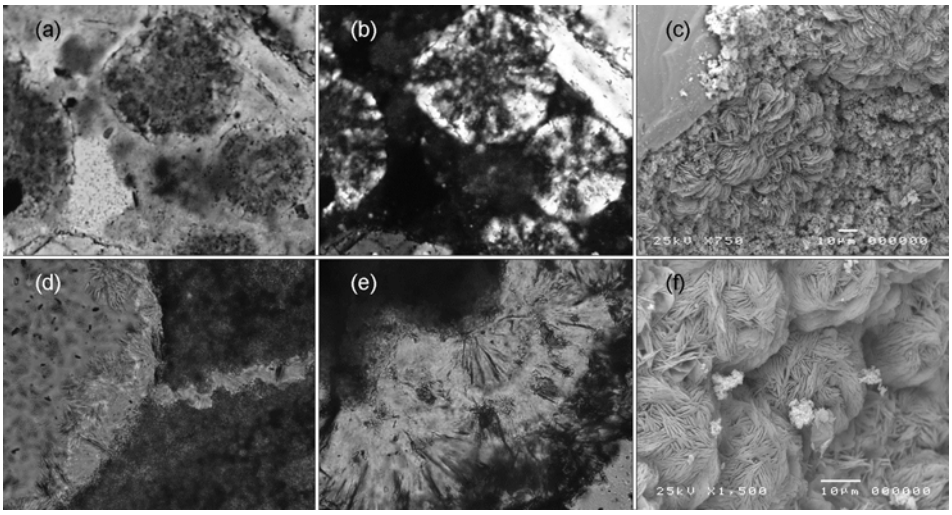


Figure 5: Examples of hydromagnesite in dolomitic lime mortars. (a) thin section photomicrograph of radial aggregate of hydromagnesite crystals in the binder; parallel polarizers, field of view 0.55 mm across; (b) the same aggregate, crossed polarizers; (c) SEM-image of hydromagnesite platelets in the binder; (d) thin section photomicrograph of hydromagnesite pore and vein fillings, parallel polarizers, field of view 0.2 mm across; (e) hydromagnesite growing on a plaster surface, parallel polarizers, field of view 0.2 mm across; (f) SEM-image of globular hydromagnesite aggregates that form as a result of undisturbed growth into open space

## 4. Discussion

As outlined in sections 3.1 and 3.2 there are significant differences in the proportions of samples containing magnesium phases, when XRD and DTA/TG results are compared. The same applies for a comparison between XRD and BSE/EMPA results. Several causes can account for this discrepancy as already mentioned in the literature (Bruni et al. 1997; Montoya et al. 2003; Siedel et. al 2003a, 2003b):

(1) The amounts of magnesium phases are below the detection limit for XRD.

(2) Magnesium phases of the binder may be present in an X-ray amorphous state due to a poor crystallinity.

(3) Compared to calcite the X-ray scattering intensity of magnesite and particularly hydromagnesite is very low. This implies that peak intensities of these phases do not reflect their real modal proportions in a sample.

By comparison, smaller amounts of magnesium phases (regardless their crystallinity) produce measurable ion currents during thermal decomposition. Compared to XRD and DTA/TG as well, the sensitivity of BSE imaging (Fig. 4b) is unsurpassed: even a single grain of a magnesium phase can be detected provided its grain size is > 3 µm. Even in case of a grain size on the order of 1 µm or below (brucite and/or magnesite and/or hitherto unidentified magnesium phases) EMPA X-ray mapping still allows the identification of magnesium in the binder matrix (Fig. 4c) albeit without an assignment to any specific phase.

## 5. Conclusion

A significant portion of the mortar and plaster samples investigated from Northern and Southern Tyrolean localities contains magnesium phases as an essential part of the binder, indicating the use of dolomite as a raw material for the binder production.

Magnesite, hydromagnesite and brucite could be identified using a combination of XRD, EMPA, Raman spectroscopy. In addition, X-ray mapping and DTA/TG analysis indicates the presence of amorphous or poorly crystalline magnesium phases.

The magnesium phase most frequently identified by XRD is magnesite. In no case was it possible to optically identify magnesite due to its invariably very small grain size and intimate intergrowth with calcite. A location of magnesite using thin section, however, is possible by combining X-ray mapping and Raman spectroscopy.

The only magnesium phase that forms large and well developed crystals is hydromagnesite. This finding contradicts earlier claims by Lanas and Alvarez (2004) that hydromagnesite does not form under conditions prevailing during setting of a dolomitic lime mortar. Even in cases in which hydromagnesite can be identified in thin sections, the modal amount of this phase can be too small to be detected with XRD.

Brucite was exclusively identified with XRD but never located in polished thin sections.

A significant portion of magnesium in the binder is present as amorphous and/or poorly crystalline (hydrous) phases.

The SEM-textures of hydromagnesite and amorphous/poorly crystalline Mg-phases typically show interlocking crystal aggregates thus indicating that these phases significantly contribute to the unusual strength and durability of medieval dolomitic lime mortars.

An unambiguous identification of magnesium phases is only possible trough a combination of several methods.

## 6. Acknowledgement

This study was carried out within the framework of an EU-Interreg-Project entitled „Interdisciplinary investigations of selected monuments as key examples for optimized planning of conservation measures." The funding for this project, provided by the European Union, the Autonomous Province of Bolzano - South Tyrol, the state of Tyrol and the Austrian ministry for education, science and culture is gratefully acknowledged.

## 7. References

Atzeni C., Massidda L. & Sanna U. 1996. Magnesian limes. Experimental contribution to interpreting historical data. Science and Technology for Cultural Heritage 5, H.2, 29-36.

Bruni S., Cariati F., Fermo P., Cairati P., Alessandrini G. & Toniolo L. 1997. White lumps in fifth- to seventeenth-century AD mortars from Northern Italy. Archaeometry, 39 (1), 1-7.

Lanas J. & Alvarez J. I. 2004. Dolomitic limes: Evolution of the slaking process under different conditions. Thermochimica Acta, 423 (1-2), 1-12.

Montoya C., Lanas J. Arandigoyen M., Navarro I., Garcia Casado P.J. & Alvarez, J.I. 2003. Study of ancient dolomitic mortars of the church of Santa Maria de Zamarce in Navarra (Spain): Comparison with simulated standards. Thermochimica Acta, 398 (1-2), 107-122.

Niesel K. & Schimmelwitz P. 1971. Zur Kenntnis der Vorgänge bei der Erhärtung und Verwitterung von Dolomitkalkmörteln. Tonind.-Zeitung 95, Nr. 6, 153–161.

Siedel H., Michalski M. & Zier H.-W. 2003a. Brennen, Löschen und Erhärten von Dolomitkalken. In: Umweltbedingte Gebäudeschäden an Denkmälern durch die Verwendung von Dolomitkalkmörteln. Abschlussbericht zum DBU-Projekt Az 15678. Institut für Steinkonservierung, Bericht Nr. 16, 7-12.

Siedel H., Michalski M., Ulrich B. & Zier H.-W. 2003b. Zur Indentifikation von Magnesiumverbindungen im Kalkmörtel. In: Umweltbedingte Gebäudeschäden an Denkmälern durch die Verwendung von Dolomitkalkmörteln. Abschlussbericht zum DBU-Projekt Az 15678. Institut für Steinkonservierung, Bericht Nr. 16, 13-20.